COMPUTED TOMOGRAPHY

"Dark-blood" dual-energy computed tomography angiography for thoracic aortic wall imaging

David C. Rotzinger[1,2] · Salim A. Si-Mohamed[3,4] · Nadav Shapira[5] · Philippe C. Douek[3,4] · Reto A. Meuli[1,2] · Loïc Boussel[3,4]

Abstract

Objectives To assess the capability of a newly developed material decomposition method from contrast-enhanced dual-energy CT images, aiming to better visualize the aortic wall and aortic intramural hematoma (IMH), compared with true non-contrast (TNC) CT.

Materials and methods Twenty-two patients (11 women; mean age, 61 ± 20 years) with acute chest pain underwent 25 dual-layer non-contrast and contrast-enhanced CT. CT-angiography images were retrospectively processed using two-material decomposition analysis, where we defined the first material as the content of a region of interest placed in the ascending aorta for each patient, and the second material as water. Two independent radiologists assessed the images from the second material termed "dark-blood" images and the TNC images regarding contrast-to-noise ratio (CNR) between the wall and the lumen, diagnostic quality regarding the presence of aortic wall thickening, and the inner/outer vessel wall conspicuity.

Results Diagnostic quality scores in normal aortic segments were 0.9 ± 0.3 and 2.7 ± 0.6 ($p < 0.001$) and wall conspicuity scores were 0.7 ± 0.5 and 1.8 ± 0.3 ($p < 0.001$) on TNC and dark-blood images, respectively. In aortic segments with IMH, diagnostic quality scores were 1.7 ± 0.5 and 2.4 ± 0.6 ($p < 0.001$) and wall conspicuity scores were 0.7 ± 0.7 and 1.8 ± 0.3 ($p < 0.001$) on TNC and dark-blood images, respectively. In normal aortic segments, CNRs were 0.3 ± 0.2 and 2.8 ± 0.9 on TNC and dark-blood images, respectively ($p < 0.001$). In aortic segments with IMH, CNRs were 0.3 ± 0.2 and 4.0 ± 1.0 on TNC and dark-blood images, respectively ($p < 0.001$).

Conclusions Compared with true non-contrast CT, dark-blood material decomposition maps enhance quantitative and qualitative image quality for the assessment of normal aortic wall and IMH.

Key Points

• *Current dual-energy CT-angiography provides virtual non-contrast and bright-blood images.*
• *Dark-blood images represent a new way to assess the vascular wall structure with dual-energy CT and can improve the lumen-to-wall contrast compared with true non-contrast CT.*
• *This dual-energy CT material decomposition method is likely to improve contrast resolution in other applications as well, taking advantage of the high spatial resolution of CT.*

Keywords Computed tomography angiography · Aorta · Hematoma · Thorax · Technology assessment

✉ David C. Rotzinger
david.rotzinger@chuv.ch

1   Department of Diagnostic and Interventional Radiology, Lausanne University Hospital (CHUV), Rue du Bugnon 46, 1011 Lausanne, Switzerland

2   Faculty of Biology and Medicine (FBM), University of Lausanne (UNIL), Lausanne, Switzerland

3   Radiology Department, Hospices Civils de Lyon (HCL), Lyon, France

4   University Claude Bernard Lyon 1, CREATIS, CNRS UMR 5220, INSERM U1206, INSA-Lyon, Lyon, France

5   CT/AMI Research and Development, Philips Medical Systems, Haifa, Israel

Abbreviations

AAS	Acute aortic syndrome
CNR	Contrast-to-noise ratio
CTA	Computed tomography angiography
DECT	Dual-energy computed tomography
HU	Hounsfield unit
IMH	Intramural hematoma
NIST	National Institute of Standards and Technology
ROI	Region of interest
TNC	True non-contrast
VNC	Virtual non-contrast

Introduction

In acute aortic syndrome (AAS), the detection of intramural hematoma (IMH) is challenging and requires a non-contrast CT acquisition in addition to CT-angiography (CTA) [1, 2]. Thanks to its ability to create virtual non-contrast (VNC) images, dual-energy CT (DECT) technology has been recently proposed to improve the detection of IMH. Nevertheless, the contrast between the aortic lumen and the vessel wall remains relatively low on VNC images and makes the detection of subtle thickening of the wall difficult [3]. Conversely, aortic magnetic resonance angiography offers the possibility to obtain "dark-blood" images by suppressing the signal of the aortic lumen and thus facilitating the depiction of the aortic wall [4] but is not generally available in emergency settings. On this same principle, we sought to develop a DECT CTA-based algorithm allowing to suppress the signal of the aortic lumen based on a modified pair material decomposition in the image domain. In this decomposition, the first material was defined as the content of a region of interest (ROI) placed in the ascending aorta, and the second material was water.

This study aimed to assess the capability of this newly developed arterial wall enhancement algorithm, termed as dark-blood imaging, to visualize the aortic wall and aortic IMH better, compared with true non-contrast (TNC) CT.

Materials and methods

Study design and patients

The institutional ethics committee approved this single-center retrospective study and waived informed consent.

We selected 25 CT examinations from 22 patients (11 men; age range, 25–89 years and 11 women; 33–86 years), referred to aortic CTA for clinically suspected AAS. From July 2017 to January 2018, all patients with IMH proven upon aortic CTA or surgery were included ($n = 11$). For those who underwent medical therapy, the diagnosis of normal aortic CTA or acute IMH was based on a consensus. Subsequently, 11 randomly selected control subjects with acute chest pain, but with normal aortic CTA, were included as well, within the same time frame. Demographics are detailed in Table 1.

Dual-layer DECT protocols and image reconstruction

All patients underwent aortic dual-layer detector DECT consisting of a TNC acquisition followed by a contrast-enhanced arterial-phase acquisition on a 64-row spectral detector CT system (IQon, Philips Healthcare). Acquisition parameters for both acquisitions were as follows: tube potential, 120 kVp; beam collimation geometry, 64×0.625 mm; gantry rotation time, 0.27 s; beam pitch, 1.234; and tube load, 55 mAs. An iodinated contrast agent (Iomeron® 400 mg I/mL, Bracco) was injected into an antecubital vein and followed by a saline flush. The acquisition was triggered by the bolus tracking technique. Reconstruction parameters were as follows: section thickness, 1.5 mm; reconstruction filter, B; iterative reconstruction algorithm, iDose 3; and display field-of-view, 300 mm.

Conventional HU images were reconstructed for the TNC acquisition. Regarding the contrast-enhanced DECT CTA acquisition, we reconstructed virtual monochromatic image series at 54 and 100 keV using the post-processing software provided with the DECT system (ISP v9.0, Philips Healthcare). The 54-keV value was chosen as the first energy level as it is sufficiently far away from the K-edge of iodine (33 keV) while being low enough to exhibit a photoelectric effect. The 100-keV value was chosen as the second energy level as it is high enough to exhibit more Compton scattering effect. We fed these two virtual monochromatic image series into a dedicated in-house software (developed using Microsoft Visual C++ 2017) to perform a two-material decomposition termed as ROI/Water (see below) and generate maps thereof. In this step, we drew an ROI in the ascending aorta on the 54-keV images and then copied and pasted it onto the 100-keV images for each patient. The mean value of these ROIs in HU was recorded and termed ROI_{54} and ROI_{100}, respectively. Then, a two-material decomposition algorithm was applied with the following method. In the (x,y) coordinate system where "x" and "y" represent the values of attenuation at 100 and 54 keV, respectively, two unit vectors were set: the first

Table 1 Patients' demographics

	IMH patients	Controls
n	11	11
Scans	14	11
Female sex (%)	45.5	54.5
Age mean ± SD (range)	74.5 ± 15.3 (43–89)	45.8 ± 14.8 (25–67)
Stanford A-type IMH (%)	45.5	None

IMH, intramural hematoma; *SD*, standard deviation

one pointing from the air point $(x,y) = (0,0)$ to the NIST-based water attenuation coefficients (υ/ρ) at 54 keV and 100 keV; the second one pointing from the air point to the (x,y) attenuation values corresponding to the ascending aorta ROI (ROI_{54} and ROI_{100}). These unit vectors were used to determine a new coordinate system termed ROI/Water axes. The value of each pixel of the monochromatic images was then represented in this new coordinate system. The magnitude of the projection on the Water axis was used to generate the dark-blood image. The projection on the ROI axis was not analyzed in this study.

Image analysis

For the qualitative analysis, we divided the aortic lumen cross-sectional area into 4 equiangular quadrants, taken on 4 pre-specified slices per patient: ascending post sinotubular segment, ascending aorta at the level of the left pulmonary artery, descending aorta at the level of the left main bronchus, and descending aorta at the level of the left atrium. Based on the presence or absence of IMH on conventional CTA, we categorized each slice as normal versus abnormal, which allowed us to evaluate the false-positive and negative rate of dark-blood images compared with TNC. Subsequently, two independent radiologists, DCR and SAS, with 6 years of experience in cardiovascular radiology reviewed dark-blood and TNC images for signs of aortic IMH on a 4-point diagnostic quality scale (3 = exemplary, 2 = diagnostic, 1 = limited, 0 = non-diagnostic), per quadrant. They also evaluated the inner and outer vessel wall conspicuity on a 3-point scale (2 = circumscribed margin, 1 = indistinct margin, 0 = obscured margin) as per the Radiologic Society of North America radiology

lexicon [5], per quadrant. Overall conspicuity was derived from the separate scores of the inner and outer wall conspicuity. The same slices served for the quantitative analysis, performed by one radiologist with 6 years of experience in cardiovascular imaging (DCR), who placed an ROI in the periaortic fat. Using the abovementioned in-house software, the same radiologist placed two concentric ROIs encompassing the aortic wall and the lumen to extract pixel values of the aortic wall. The observer noted the mean and standard deviation of the voxels' value in each ROI (in HU) and calculated the contrast-to-noise ratio (CNR) between the wall and the lumen and between the wall and the periaortic fat, on both dark-blood and TNC images using the following formula:

$$CNR = \frac{\left|\text{mean ROI value}_{wall} - \text{mean ROI value}_{tissue}\right|}{\sqrt{\frac{1}{2}\left(SD_{wall}^2 + SD_{tissue}^2\right)}}$$

where the subscript "tissue" refers to mean ROI values in the aortic lumen and periaortic fat, respectively, and "wall" refers to the ROI values of the aortic wall. We also extracted the mean vessel wall thickness for each patient using our in-house software, on dark-blood images.

Quantitative variables are presented as mean and standard deviation unless stated otherwise. Statistical analysis was conducted using R (R v. 3.4.3, R Foundation for Statistical Computing), using the Wilcoxon-Mann-Whitney test to compare ordinal and continuous variables, as the data was not normally distributed according to the Shapiro-Wilk test. Interrater agreement was evaluated using the weighted kappa test. One observer repeated the evaluation 1 week later to assess intra-observer agreement, using the weighted kappa

Fig. 1 Healthy patient (a–c) and patient with a Stanford A-type intramural hematoma (d–f). Note the enhanced visibility of the aortic vessel wall on dark-blood material decomposition (b and e), as compared to the true non-contrast (a and d) and arterial-phase contrast-enhanced images (c and f)
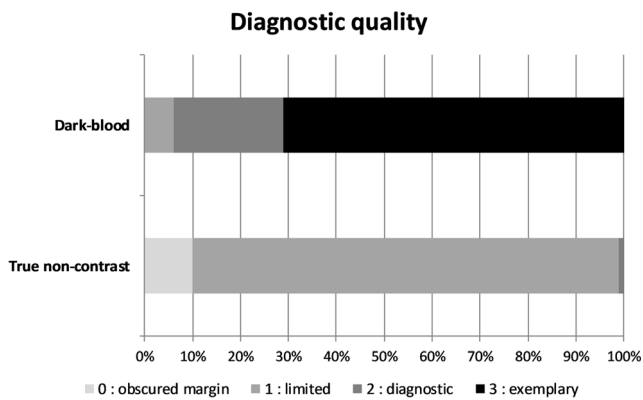
Diagnostic quality
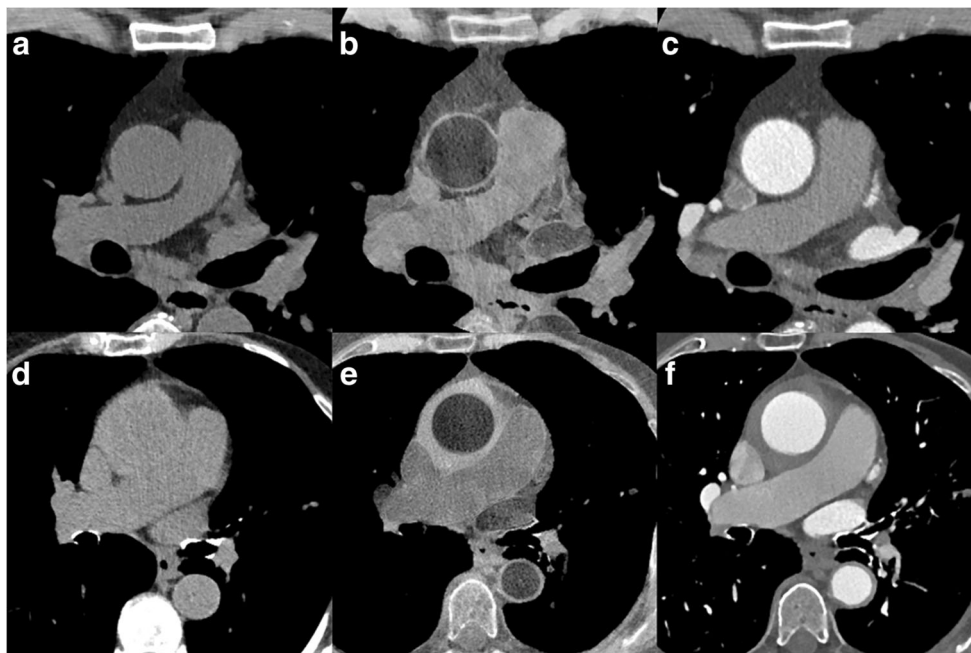
Fig. 2 Bar graph shows qualitative diagnostic quality mean scores of observers. Dark-blood images were mostly rated diagnostic or exemplary, while true non-contrast images were mostly rated limited
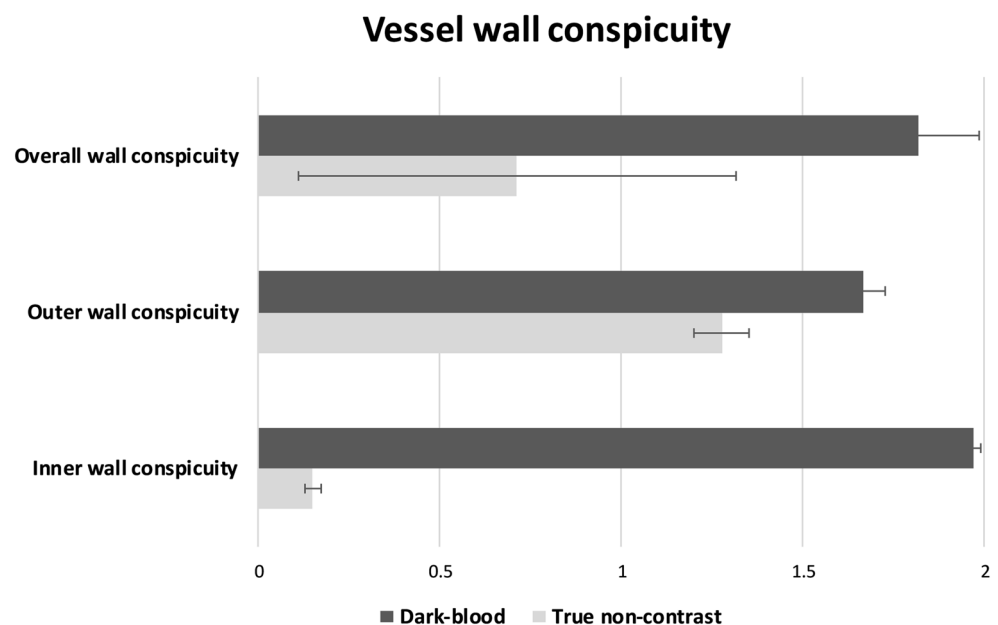
test. P values of less than 0.05 were considered statistically significant.

Results

Two typical examples of TNC, dark-blood, and conventional CTA images are provided in Fig. 1, in a control subject and a patient suffering from Stanford A-type IMH. In both cases, dark-blood images provide improved visualization of the aortic vessel wall structure.

Qualitative diagnostic quality scores in normal aortic segments were 0.9 ± 0.3 and 2.7 ± 0.6 on TNC and dark-blood images, respectively ($p < 0.001$). Aortic vessel wall conspicuity scores were 0.7 ± 0.5 and 1.8 ± 0.3 on TNC and dark-blood images, respectively ($p < 0.001$). Similarly, in aortic segments with IMH, the diagnostic quality scores were 1.7 ± 0.5 and 2.4 ± 0.6 on TNC and dark-blood images, respectively

($p < 0.001$). Aortic vessel wall conspicuity scores were 0.7 ± 0.7 and 1.8 ± 0.3 on TNC and dark-blood images, respectively ($p < 0.001$). The intra-rater agreement was substantial (weighted kappa = 0.77 and 0.71 for diagnostic quality and aortic wall conspicuity, respectively). The interrater agreement was substantial (weighted kappa = 0.74 and 0.66 for diagnostic quality and aortic wall conspicuity, respectively). Average qualitative diagnostic quality scores, including both IMH patients and control subjects, are shown in Fig. 2, and average vessel wall conspicuity scores, including both IMH patients and control subjects, are shown in Fig. 3. Finally, dark-blood images did not lead to false-positives or negatives for IMH identification.

In the quantitative analysis (Fig. 4), normal aortic segment CNRs between the vessel wall and lumen were 0.3 ± 0.2 and 2.8 ± 0.9 on TNC and dark-blood images, respectively ($p < 0.001$); CNRs between the vessel wall and the periaortic fat were 9.5 ± 2.6 and 2.6 ± 1.2 on TNC and dark-blood images, respectively ($p < 0.001$). Similarly, in aortic segments with IMH, CNRs between the vessel wall and lumen were 0.3 ± 0.2 and 4.0 ± 1.0 on TNC and dark-blood images, respectively ($p < 0.001$); CNRs between the vessel wall and the periaortic fat were 11.2 ± 4.5 and 4.7 ± 1.5 on TNC and dark-blood images, respectively ($p < 0.001$). Finally, mean aortic vessel wall thickness was 1.6 ± 0.3 mm in normal segments and 4.7 ± 2.3 mm in segments with IMH ($p < 0.001$).

Discussion

Our results indicate that contrast-enhanced DECT-derived dark-blood CT imaging is feasible and may facilitate the analysis of arterial vessel walls.

Fig. 3 Qualitative analysis of vessel conspicuity on a 3-point Likert scale (2 = circumscribed margin, 1 = indistinct margin, 0 = obscured margin). Bar graph represents mean scores of observers one and two. Overall conspicuity is the average of outer and inner wall conspicuity. Error bars represent standard deviation

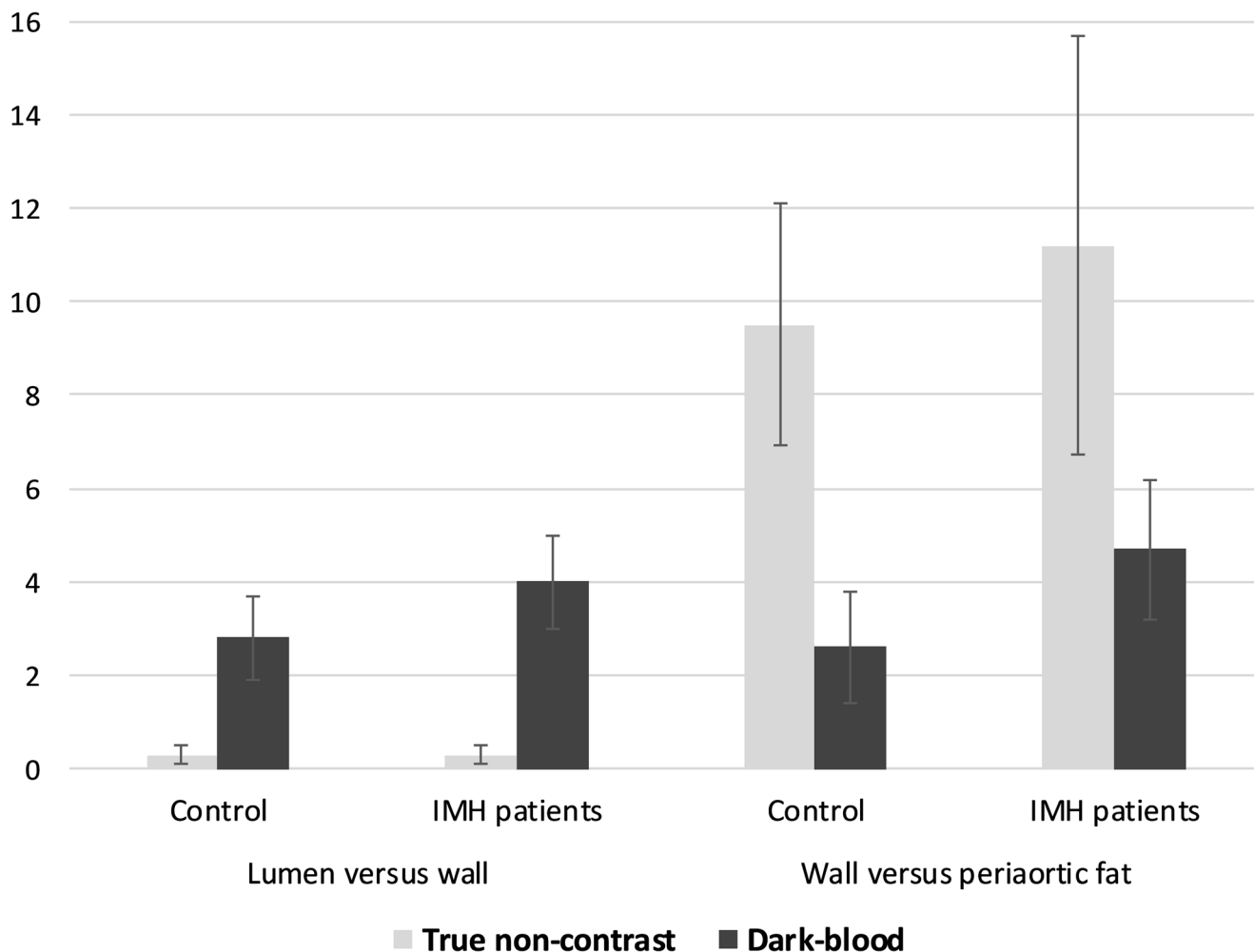## Vessel wall conspicuity

Contrast-to-noise ratio

Fig. 4 Bar graph shows contrast-to-noise ratios (CNR) obtained on true non-contrast and dark-blood images. CNR was calculated between the aortic vessel wall and lumen, as well as between vessel wall and periaortic fat, in control subjects and patients with intramural hematoma (IMH). Error bars represent standard deviation. Dark-blood images improve CNR between the lumen and the aortic wall but offer no advantage in wall versus periaortic fat CNR

In our study, dark-blood CT images significantly improved arterial wall conspicuity, resulting in better qualitative diagnostic quality. Results from the quantitative image analysis mostly support the qualitative analysis, demonstrating improved CNR between the vessel wall—with or without IMH—and the vessel lumen. Nevertheless, CNR between the vessel wall and periaortic fat was substantially lower in dark-blood images, as compared to TNC, but these results hold only as long as the aorta is indeed surrounded by fat. The aorta may be in close proximity to many organs. The reason why the observers gave better scores to the outer vessel wall delineation on dark-blood images probably comes from the impact of the material decomposition on adjacent vascular structures, such as the superior vena cava, the pulmonary artery, or any additional contrast medium–containing blood vessels, helping to demarcate the outer aortic contour. Finally, the

mean aortic wall thickness in healthy patients was approximately 1.6 mm, which is in agreement with MRI studies [6].

Regarding the method to calculate the dark-blood images, our main idea was to use a traditional two-material water/iodine decomposition, but to replace the iodine component by a value directly measured in the aortic lumen. Indeed, the exact concentration and composition of the elements present in the lumen is unknown and represents a patient and contrast material injection-dependent mixture of iodine, hemoglobin, water, platelets, and other components. By directly using the attenuation measured in the aortic lumen, we calibrated the slope of the non-water axis used for the two-material decomposition and thus accurately canceled the attenuation of the lumen on the water axis used to generate the dark-blood images. It is important to notice that, with our method, we directly used the HU values measured in the aortic lumen on the

two monochromatic images (i.e., 54 and 100 keV) and did not unscale them to their physical attenuation values. This results in an additional scaling factor, which in fact is also dependent on the measured HU values of the aortic lumen. The geometric interpretation of this scaling factor can be seen as a decrease in the slope of the calibrated aortic lumen material, resulting in negative calculated projections along the water material for the aortic lumen values. As a consequence, the two-material decomposition we applied does not result in concentration maps but rather in a map of geometric projections that allow for optimized contrast between the lumen and the surrounding tissues, while keeping a contrast between the surrounding tissues themselves. Unfortunately, despite their added value for visualization, these projection maps do not have any meaningful physical interpretation and are not intended to be a quantitative method. An analogy can be performed with MRI. The absolute T1 of the tissue can be measured with MRI to create T1 maps, commonly used in cardiac MRI, for example [7]. However, most of the time, T1-weighed images are used, where the contrast relies on the differences in T1 between tissues consisting of unknown elements, such as performed with our method in DECT.

Our study highlights the potential benefit of dark-blood aortic CT imaging compared with the current state-of-the-art aortic CT imaging, usually consisting of TNC CT followed by CTA [8]. As of today, TNC CT combined with CTA is still recommended for suspected AAS patients. CTA alone may provide inferior diagnostic accuracy [1] due to the high luminal attenuation that can mask the IMH, as CTA requires wide window settings to display images [9–11]. This two-acquisition approach increases the total examination radiation dose. Furthermore, TNC CT results in a low visual contrast between the vessel wall and the lumen it provides, causing interpretive difficulties in assessing structural changes in the vessel wall. In this context, dark-blood CT images could potentially overcome these current protocol limitations by providing high wall-to-lumen contrast form a single contrast-enhanced acquisition. This last statement would need a more extensive study, involving more patients, which was beyond the scope of the present feasibility study.

Our study has several limitations. First, a true blinded design was not achievable given the unique nature of dark-blood images compared to TNC. Then, the comparison between dark-blood images and other results available from spectral CTA, such as HU or different levels of monochromatic images, in IMH but also in other conditions leading to acute aortic syndrome, has not been performed in this study. This would certainly be of interest but was beyond the scope of the present study.

In conclusion, we describe a dark-blood image decomposition method that provides a new way to show contrast between tissues. We took the example of producing dark-blood CT images of the aorta to visualize the vessel wall, to help diagnose conditions associated with changes in the vessel wall structure, compared with TNC. The same method may improve contrast resolution in other applications.

Compliance with ethical standards

Guarantor The scientific guarantor of this publication is Prof. Philippe C. Douek, MD, PhD.

Conflict of interest The authors of this manuscript declare relationships with the following companies: Dr. Nadav Shapira, PhD, is employed by Philips Healthcare, the manufacturer of the DECT system used in this study.

Statistics and biometry No complex statistical methods were necessary for this paper.

Informed consent Written informed consent was waived by the Institutional Review Board.

Ethical approval Institutional Review Board approval was obtained.

Methodology
• retrospective
• cross-sectional study
• performed at one institution

References

1. Lemos AA, Pezzullo JC, Fasani P et al (2014) Can the unenhanced phase be eliminated from dual-phase CT angiography for chest pain? Implications for diagnostic accuracy in acute aortic intramural hematoma. AJR Am J Roentgenol 203:1171–1180

2. Erbel R, Aboyans V, Boileau C et al (2014) 2014 ESC Guidelines on the diagnosis and treatment of aortic diseases: Document covering acute and chronic aortic diseases of the thoracic and abdominal aorta of the adult. The Task Force for the Diagnosis and Treatment of Aortic Diseases of the European Society of Cardiology (ESC). Eur Heart J 35:2873–2926

3. Lehti L, Söderberg M, Höglund P, Nyman U, Gottsäter A, Wassélius J (2018) Reliability of virtual non-contrast computed tomography angiography: comparing it with the real deal. Acta Radiol Open 7:205846011879011

4. Simonetti OP, Finn JP, White RD, Laub G, Henry DA (1996) "Black blood" T2-weighted inversion-recovery MR imaging of the heart. Radiology 199:49–57

5. RSNA RadLex radiology lexicon. http://radlex.org/. Accessed 14 Jun 2018

6. Mensel B, Kühn JP, Schneider T et al (2013) Mean thoracic aortic wall thickness determination by cine MRI with steady-state free precession: validation with dark blood imaging. Acad Radiol 20: 1004–1008

7. Burt JR, Zimmerman SL, Kamel IR, Halushka M, Bluemke DA (2014) Myocardial T1 mapping: techniques and potential applications. Radiographics 34(2):377–395

8. Gutschow SE, Walker CM, Martínez-Jiménez S, Rosado-de-Christenson ML, Stowell J, Kunin JR (2016) Emerging concepts in intramural hematoma imaging. Radiographics 36:660–674

9. Manghat NE, Morgan-Hughes GJ, Roobottom CA (2005) Multi-detector row computed tomography: imaging in acute aortic syndrome. Clin Radiol 60:1256–1267

10. Holloway BJ, Rosewarne D, Jones RG (2011) Imaging of thoracic aortic disease. Br J Radiol 84(Spec No 3):S338–S354

11. Zatz LM (1981) Basic principles of computed tomography scanning. In: Newton TH, Potts DG (eds) Technical aspects of computed tomography. Mosby, St. Louis, pp 3853–3876